

Cell Metabolism, Volume 20

## Supplemental Information

### Estradiol Regulates Brown Adipose Tissue

#### Thermogenesis via Hypothalamic AMPK

Pablo B. Martínez de Morentin, Ismael González-García, Luís Martins, Ricardo Lage, Diana Fernández-Mallo, Noelia Martínez-Sánchez, Francisco Ruíz-Pino, Ji Liu, Donald A. Morgan, Leonor Pinilla, Rosalía Gallego, Asish K. Saha,0 Andries Kalsbeek, Eric Fliers, Peter H. Bisschop, Carlos Diéguez, Rubén Nogueiras, Kamal Rahmouni, Manuel Tena-Sempere, and Miguel López

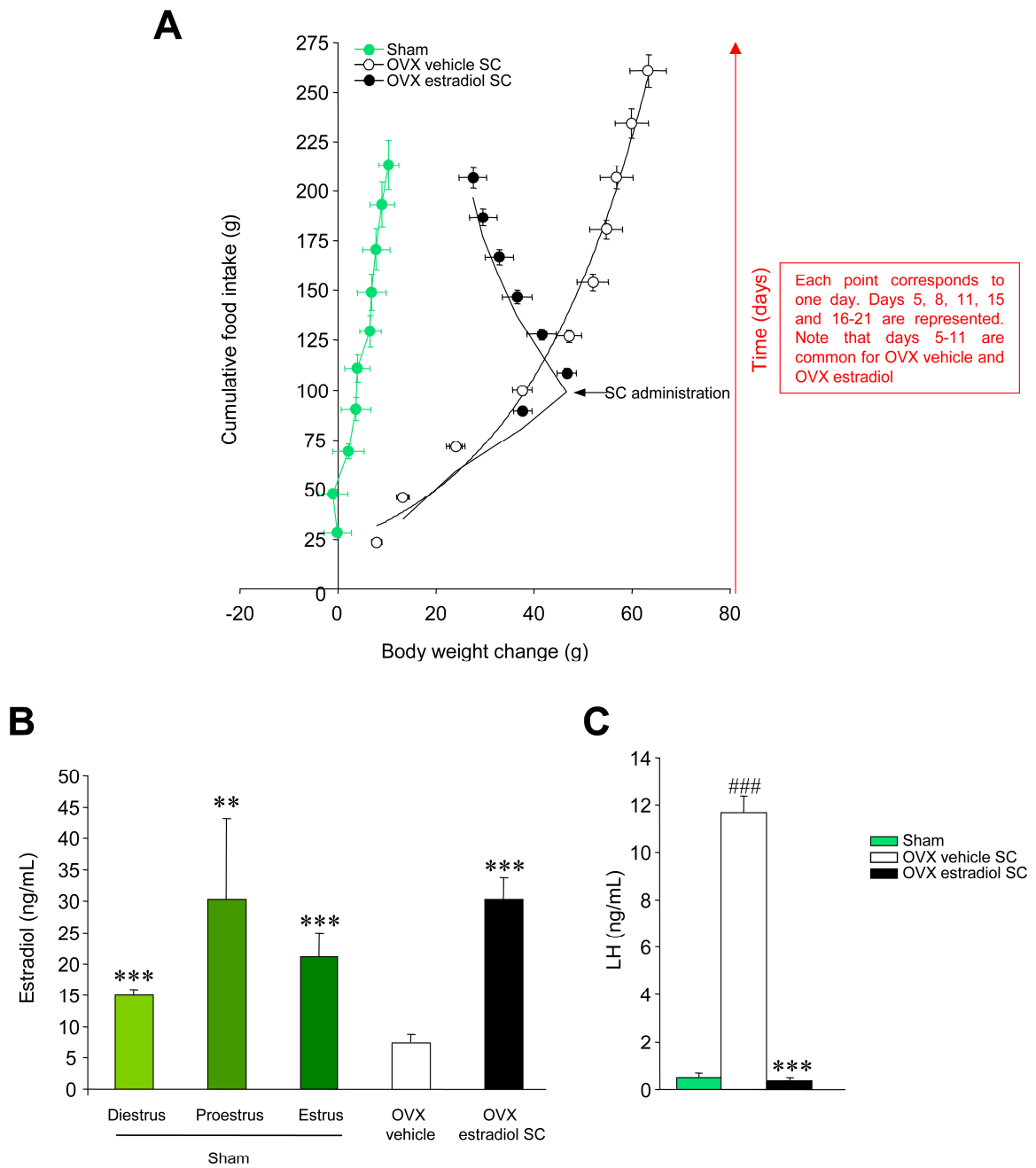


**FIGURE S1, related to Figure 1. Effect of peripheral E2 treatment on energy balance and plasma E2 and LH levels.**

**(A)** Energy balance plot, **(B)** plasma E2 levels (for sham rats in different stages of the estrus cycle) and **(C)** plasma luteinizing hormone (LH) levels of sham and OVX rats SC treated with vehicle or E2. Error bars represent SEM;  $n=7-19$  animals per experimental group. \*\* and \*\*\* $P<0.01$  and  $0.001$  vs. OVX E2 SC; ### $P<0.001$  vs. sham.

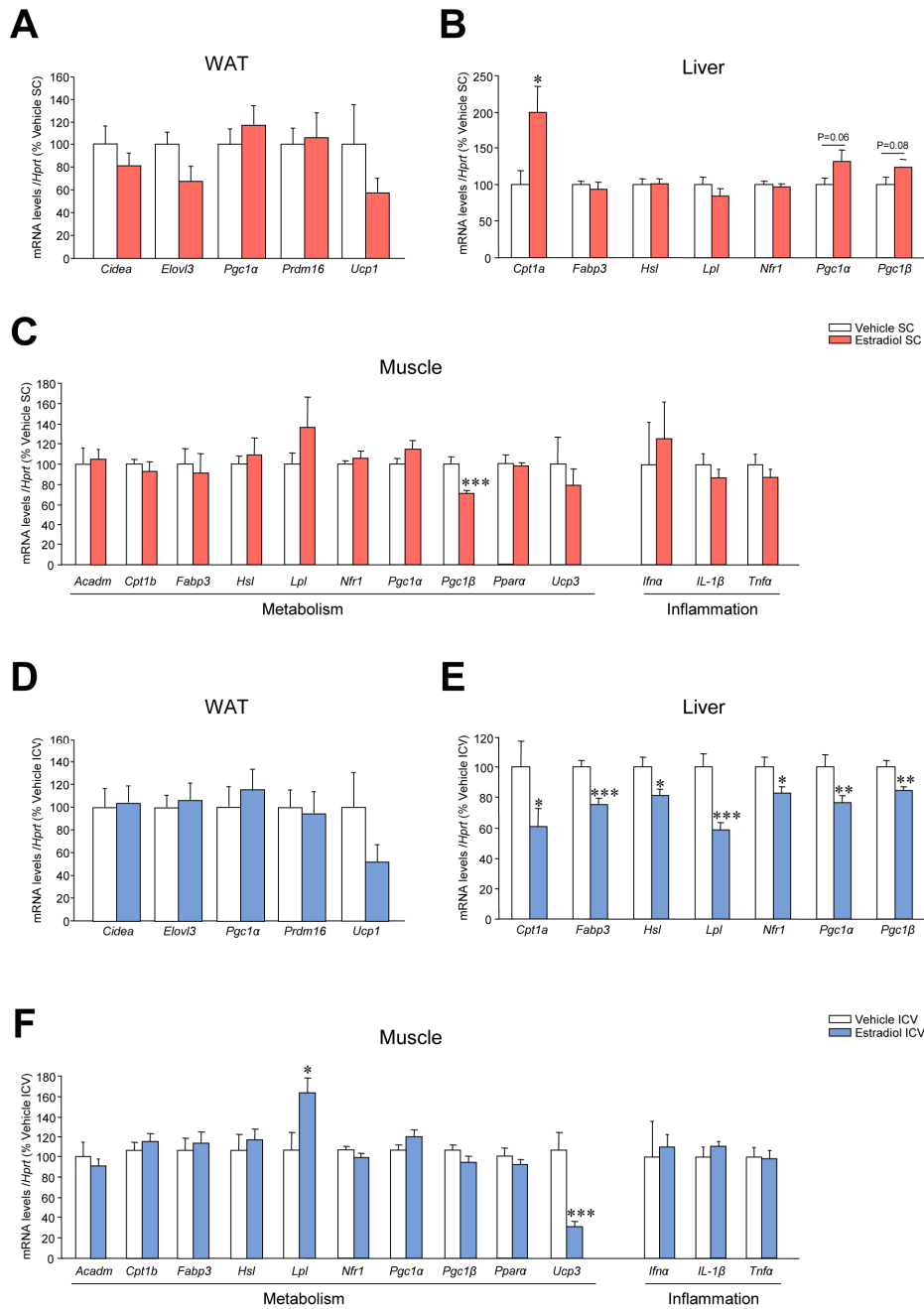


**FIGURE S2, related to Figure 2. Effect of peripheral or central E2 treatment on browning markers in WAT and metabolic and inflammatory markers in liver and muscle.**

mRNA profiles in WAT (A), liver (B) and muscle (C) of OVX rats treated SC with vehicle or E2. mRNA profiles in WAT (D), liver (E) and muscle (F) of OVX rats treated ICV with vehicle or E2. Error bars represent SEM; n= 7-9 animals per experimental group. \*, \*\* and \*\*\*P<0.05, 0.01 and 0.001 vs. vehicle (SC or ICV).

**A**

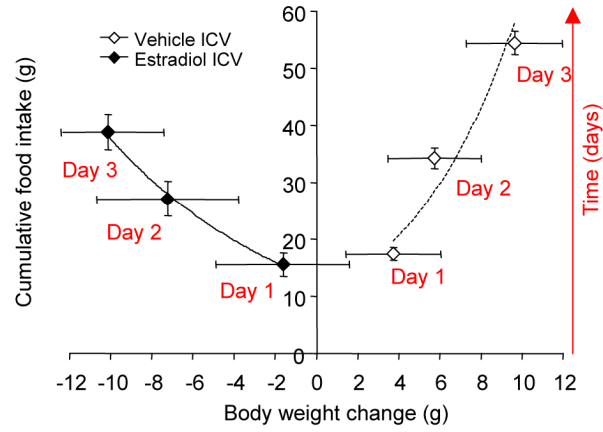


**FIGURE S3, related to Figure 3. Effect of central E2 treatment on energy balance.**

**(A)** Energy balance plot of rats treated with vehicle or E2. Error bars represent SEM; n= 12 animals per experimental group.

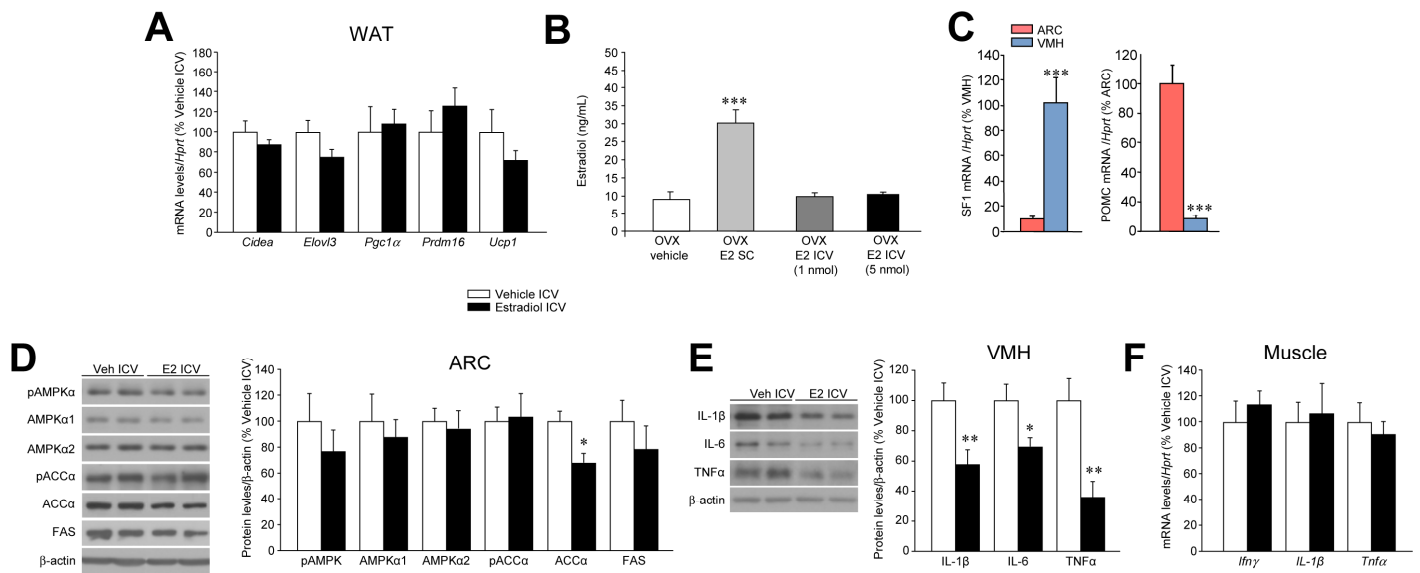


**FIGURE S4, related to Figure 4. Effect of central E2 treatment on WAT browning program, ARC AMPK pathway and hypothalamic and muscle inflammation.**

(A) Browning markers in WAT of OVX rats ICV treated with vehicle or E2. (B) Plasma E2 levels of OVX rats SC and ICV treated with vehicle or E2. (C) SF1 and POMC mRNA levels in VMH and ARC dissections. (D) Western blot autoradiographic images (left panel) and protein levels of the AMPK pathway in the ARC (right panel) of OVX rats ICV treated with vehicle or E2. (E) Western blot autoradiographic images (left panel) and protein levels of inflammatory markers (right panel) in the VMH of rats ICV treated with vehicle or E2. (F) mRNA levels of inflammatory markers in muscle of OVX rats ICV treated with vehicle or E2. Error bars represent SEM; n=7-19 animals per experimental group. \*, \*\* and \*\*\*P<0.05, 0.01 and 0.001 vs. vehicle ICV.

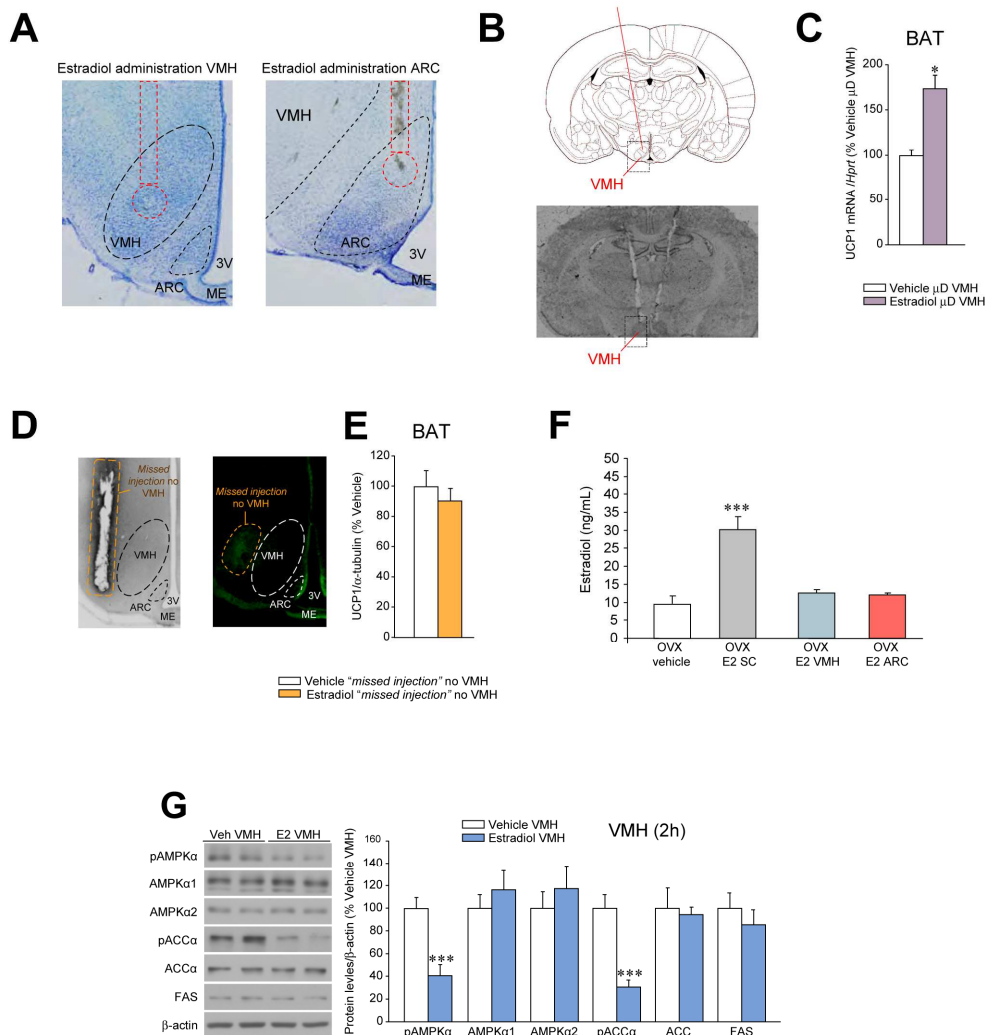


**FIGURE S5, related to Figure 5. Histological and expression controls of E2 administration into the VMH.**

(A) Representative photomicrographs (10X) of toluidine blue staining of brain sections from rats treated with E2 in the VMH or the ARC. The injection route is enclosed in a red rectangle and the injection place in a red circle. (B) Schematic representation (from *Paxinos and Watson Rat Brain Atlas*; upper panel) and representative photomicrograph of brain sections showing the injection route for microdialysis (lower panel) and (C) UCP1 mRNA levels in BAT of OVX rats treated by microdialysis with vehicle or E2 within the VMH. (D) Representative photomicrographs of brain sections (4X) showing "missed" injections in "VMH neighboring" areas in OVX rats. (E) BAT UCP1 protein levels of OVX rats with "missed" injections in "VMH neighboring" areas. (F) Plasma E2 levels of OVX rats SC, VMH or ARC treated with E2. (G) Western blot autoradiographic images (left panel) and protein levels of the AMPK pathway in the VMH (right panel) of OVX rats stereotaxically treated with vehicle or E2 within the VMH for 2 hours. Error bars represent SEM; n=6-19 animals per experimental group. \*P<0.05 vs. vehicle  $\mu$ D VMH and \*\*\*P<0.001 vs. OVX vehicle or vehicle VMH.

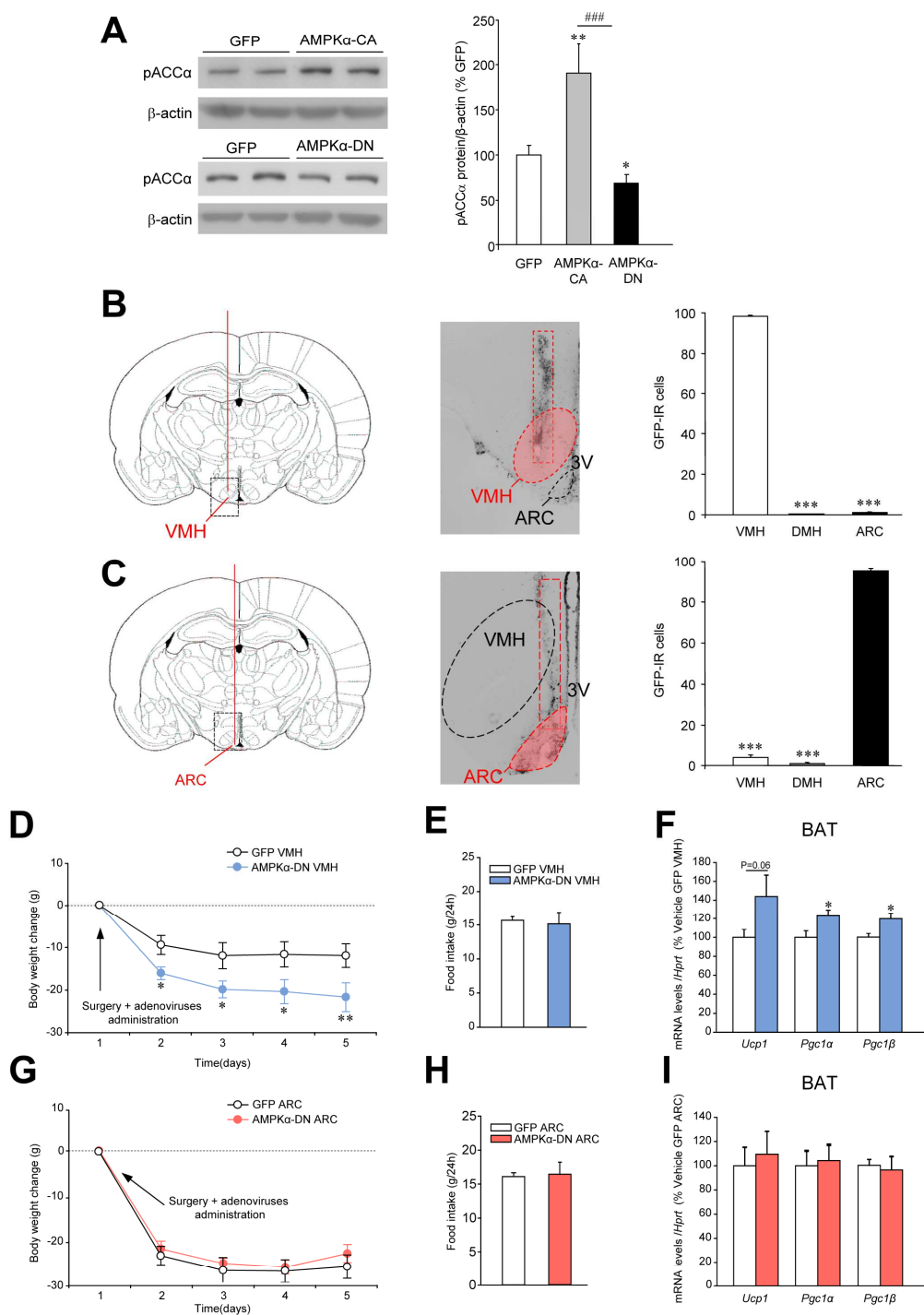


**FIGURE S6, related to Figure 6. Histological and expression controls of AMPKα adenoviruses administration into the VMH and ARC. Effect of inactivation of hypothalamic AMPK in OVX rats on energy balance.**

**(A)** Western blot autoradiographic images (left panel) and hypothalamic protein levels of pACCα (right panel) of rats stereotaxically treated with adenoviruses encoding GFP, AMPKα-CA and AMPKα-DN. **(B)** Schematic representation (from *Paxinos and Watson Rat Brain Atlas*, left panel), representative photomicrograph of brain sections (central panel) showing the injection route for stereotaxic administration and GFP-immunopositive cells (right panel) of rats treated with AMPKα adenoviruses into the VMH. **(C)** Schematic representation (from *Paxinos and Watson Rat Brain Atlas*, left panel), representative photomicrograph (central panel) showing the injection route for stereotaxic

administration and GFP-immunopositive cells (right panel) of rats treated with AMPK $\alpha$  adenoviruses into the ARC. **(D)** Body weight, **(E)** daily food intake and **(F)** mRNA expression profile in the BAT of OVX rats stereotaxically treated with GFP or AMPK $\alpha$ -DN adenoviruses into the VMH. **(G)** Body weight, **(H)** daily food intake and **(I)** mRNA expression profile in the BAT of OVX rats stereotaxically treated with GFP or AMPK $\alpha$ -DN adenoviruses into the ARC. Error bars represent SEM; n= 8 animals per experimental group. 3V: third ventricle; \*P<0.05 vs. GFP or GFP VMH; \*\*P<0.01 vs. GFP; \*\*\*P<0.001 vs. VMH or ARC (panels B and C); ###P<0.01 vs. AMPK $\alpha$ -DN

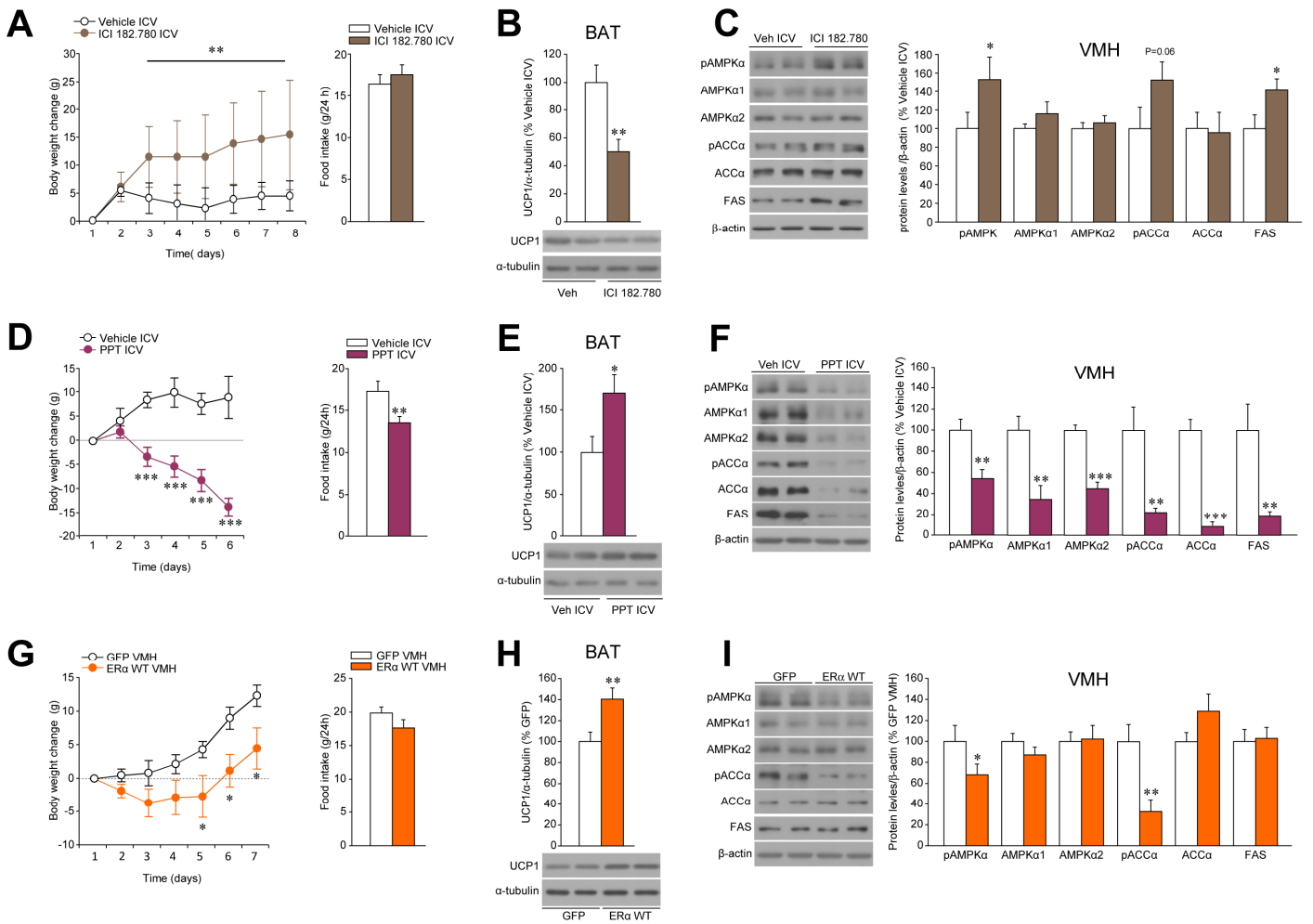


**FIGURE S7, related to Figure 7. Effect of pharmacological and genetic modulation of estrogen receptor alpha (ER $\alpha$ ) over energy balance.**

**(A)** Body weight change (left panel) and daily food intake (right panel), **(B)** protein levels (upper panel) and western blot autoradiographic images of BAT UCP1 protein (lower panel) and **(C)** western blot autoradiographic images (left panel) and protein levels of the AMPK pathway in the VMH (right panel) of intact rats ICV treated with the combined ER $\alpha$ - $\beta$  antagonist ICI 182.780. **(D)** Body weight change (left panel) and daily food intake (right panel), **(E)** protein levels (upper panel) and western blot autoradiographic images of BAT UCP1 protein (lower panel) and **(F)** western blot autoradiographic images (left panel) and protein levels of the AMPK pathway in the VMH (right panel) of OVX rats ICV treated with the specific ER $\alpha$  agonist PPT. **(G)** Body weight change (left panel) and daily food intake (right panel), **(H)** protein levels (upper panel) and western blot autoradiographic images of BAT UCP1 protein (lower panel) and **(I)** western blot autoradiographic images (left panel) and protein levels of the AMPK pathway in the VMH (right panel) of OVX rats stereotactically treated within the VMH with adenovirus encoding a wildtype (WT) isoform of ER $\alpha$ . Error bars represent SEM; n=7-8 animals per experimental group. \*, \*\* and \*\*\* P<0.05, 0.01 and 0.001 vs. vehicle ICV or GFP VMH.

**Table S1:** Primers and probes for real-time PCR analysis

<i>mRNA</i>	Gene name	GenBank Accession number		Sequence
<i>Acadm</i>	Acyl-CoA dehydrogenase	NM_016986.2	Fw Primer Rv Primer Probe	5'-GCCTTCACCGGATTCATCGT-3' 5'-GCACCGCTGACCCATGTT-3' 5'-FAM- CCCGGAATACACATCGGAAAAAGGAACT-3'
<i>Cidea</i>	Cell death-inducing DFFA-like effector a	NM_001170467.1	Assay ID	Applied Biosystems TaqMan® Gene Expression Assays Assay ID Rn04181355_m1
<i>Cpt1a</i>	Carnitine palmitoyltransferase 1a, (liver)	NM_031559.1	Fw Primer Rv Primer Probe	5'-ATGACGGCTATGGTGTCTCC-3' 5'-TCATGGCTTGCTTCAAGTGC-3' FAM-5'-TGAGACAGACTCACACCGCT-3'- TAMRA
<i>Cpt1b</i>	Carnitine palmitoyltransferase 1b, (muscle)	NM_013200	Assay ID	Applied Biosystems TaqMan® Gene Expression Assays Assay ID Rn01407782_g1
<i>Elovl3</i>	Fatty acid elongase 3	NM_001107602.1	Assay ID	Applied Biosystems TaqMan® Gene Expression Assays Assay ID Rn01411024_m1
<i>Fabp3</i>	Fatty acid binding protein 3	NM_024162	Fw Primer Rv Primer Probe	5'-ACGGAGGCAAACCTGGTCCAT-3' 5'-CACTTAGTTCCTGTAAGCGTAGTC-3' FAM-5'-TGCAGAAGTGGGACGGGCAGG-3'- TAMRA
<i>Hprt</i>	Hypoxanthine phosphoribosyltransferase 1	NM_012583	Fw Primer Rv Primer Probe	5'-AGCCGACCGTTCTGTCAT-3' 5'-GGTCATAACCTGGTTCATCATCAC -3' FAM-5'- CGACCCTCAGTCCCAGCGTCGTGAT 3'-TAMRA
<i>Hsl</i>	Lpase, hormone sensitive (Lipe)	NM_012859	Fw Primer Rv Primer Probe	5'-CCAAGTGTGTGAGCGCCTATT -3' 5'-TCACGCCCAATGCCTTCT -3' FAM-5'- AGGGACAGAGACGGAGGACCATTTTGACTC - 3'-TAMRA
<i>Ifny</i>	Interferon gamma	NM_138880.2	Assay ID	Applied Biosystems TaqMan® Gene Expression Assays Assay ID Rn00594078_m1
<i>Il-1β</i>	Interleukin 1 beta	NM_031512.2	Assay ID	Applied Biosystems TaqMan® Gene Expression Assays Assay ID Rn00580432
<i>Lpl</i>	Lipoprotein lipase	NM_012598	Fw Primer Rv Primer Probe	5'-CTGAAAGTGAGAACATTCCCTTCA-3' 5'-CCGTGTAAATCAAGAAGGAGTAGGTT-3' FAM-5'-CCTGCCGGAGGTCGCCACAAATA-3'- TAMRA
<i>Nrf-1</i>	Nuclear respiratory factor 1	NM_001100708.1	Fw Primer Rv Primer Probe	5'-TGTTTGGCGCAGCACCTTT-3' 5'-CGC AGA CTC CAG GTC TTC CA-3' FAM-5'- ATGTGGTGCGCAAGTACAAGAGCATGATC3'-

<i>Pdrm16</i>	PR domain containing 16	NM_001177995.1	Assay ID	TAMRA Applied Biosystems TaqMan® Gene Expression Assays Assay ID Mm01266512_m1
<i>Pgc1a</i>	Peroxisome proliferator-activated receptor gamma, coactivator 1 alpha (Ppargc1a)	NM_031347	Fw Primer Rv Primer Probe	5'-CGATCACCATATTCCAGGTCAAG-3' 5'-CGATGTGTGCGGTGTCTGTAGT -3' 5'-AGGTCCCCAGGCAGTAGATCCTCTTCAAGA -3'
<i>Pgc1β</i>	Peroxisome proliferator-activated receptor gamma, coactivator 1 beta (Ppargc1b)	NM_176075	Assay ID	Applied Biosystems TaqMan® Gene Expression Assays Assay ID Rn00598552_m1
<i>Pomc</i>	Proopiomelanocortin		Fw Primer Rv Primer Probe	5'-CGTCCTCAGAGAGCTGCCTTT-3' 5'-TGTAGCAGAATCTCGGCATCTTC-3' FAM-5'-CGCGACAGAGCCTCAGCCACC-3'-TAM
<i>Ppara</i>	Peroxisome proliferator activated receptor alpha	NM_013196.1	Fw Primer Rv Primer Probe	5'-TGGAGTCCACGCATGTGAAG-3' 5'-CGCCAGCTTTAGCCGAATAG-3' 5'-FAM-CTGCAAGGGCTTCTTTTCGGCGA-3' 5'-CAATGACCATGTACACCAAGGAA-3'
<i>Ucp1</i>	Uncoupling protein 1	NM_012682	Fw Primer Rv Primer Probe	5'-GATCCGAGTCGCAGAAAAGAA-3' FAM-5'-ACCGGCAGCCTTTTTCAAAGGGTTTG-3'-TAMRA
<i>Ucp3</i>	Uncoupling protein 3	NM_013167.2	Fw Primer Rv Primer SYBR green	5'-AATCAGCTTTGCTTCCCTCA-3' 5'-GCT TTGTGCTTGCATTCTGA-3'
<i>Sf-1</i>	Steroidogenic factor 1		Assay ID	Applied Biosystems TaqMan® Gene Expression Assays Assay ID Rn00565874_m1
<i>Tnfa</i>	Tumor necrosis factor alpha	NM_012675.3	Assay ID	Applied Biosystems TaqMan® Gene Expression Assays Assay ID Rn00584298_m1
			Fw Primer Rv Primer Probe	5'-CTAACTCCCAGAAAAGCAAGCAA-3' 5'-CCTCGGGCCAGTGTATGAGA-3' 5'-FAM-CAGCCAGGCAGGTTCCGTCC-3'

---

## **SUPPLEMENTAL EXPERIMENTAL PROCEDURES**

### **Determination of estrus cycle stages**

Female rats were monitored for estrus cycle by daily vaginal cytology, and only rats with at least two consecutive regular 4-days estrus cycles were used in expression analyses, as previously reported (Vigo et al., 2007).

### **Implantation of intracerebroventricular cannulae**

Chronic intracerebroventricular (ICV) cannulae were implanted under ketamine/xylazine anesthesia, as described previously and correct positioning in the lateral ventricle was confirmed by postmortem histological examination (López et al., 2008; López et al., 2010; Martínez de Morentin et al., 2012; Whittle et al., 2012). The animals were caged individually and used for experimentation four days later. During this post-operative recovery period the rats became accustomed to the handling procedure under non-stressful conditions.

### **Implantation of microdialysis probes and central treatments**

Rats were placed in a stereotaxic frame (*David Kopf Instruments*; Tujunga, CA, USA) under ketamine/xylazine anesthesia. Bilateral microdialysis probes were placed in the VMH as previously reported (Liu et al., 2013). The coordinates for the ICV probe were AP: 0.6mm, lateral: 1.5mm and ventral 3.5mm from the surface of the dura and for the VMH AP: 2.5mm, lateral: 2.0mm (angled at 10°) and 9.0 mm ventral from the dura. Microdialysis probes were implanted 1-week before the start of the experiment. The day before the experiment animals were connected to a metal collar which was kept out of reach from the rats by means of a counterbalanced beam. This allowed all manipulations to be performed outside the cages without handling the animals. 1 mg of 17 $\beta$ -estradiol

(17 $\beta$ -E2; *Sigma*; St. Louis, MO, USA) was dissolved in 1 ml pure DMSO and diluted 100 times with Ringer solution. Ringer's dialysis (3 $\mu$ l/min) in the VMH via the microdialysis probes was started at t=-60 min. At t=0 min 17 $\beta$ -E2 (10  $\mu$ g/ml, 3  $\mu$ l/min) or vehicle (Ringer with 1% DMSO, 3  $\mu$ l/min) were infused by retrodialysis into VMH during a period of 180 min.

### **Stereotaxic microinjection**

Rats treated with vehicle or E2 were placed in a stereotaxic frame (*David Kopf Instruments*; Tujunga, CA, USA) under ketamine/xylazine anesthesia. The ARC and the VMH were targeted bilaterally using a 25-gauge needle (*Hamilton*; Reno, NV, USA). The injections were directed to the following stereotaxic coordinates: *a*) for the VMH: 2.4/3.2 mm posterior to the bregma (two injections were performed in each VMH),  $\pm$ 0.6 mm lateral to midline and 10.1 mm ventral; *b*) for the ARC -2.8 mm posterior (one injection was performed in each ARC),  $\pm$ 0.3 mm lateral to bregma and 10.2 mm ventral, as previously reported (López et al., 2008; López et al., 2010; Martínez de Morentin et al., 2012; Whittle et al., 2012). Viral vectors were delivered at a rate of 200 nl/min for 5 min (1  $\mu$ l/injection site) as previously reported (López et al., 2008; López et al., 2010; Martínez de Morentin et al., 2012; Whittle et al., 2012).

### **Sample processing**

In central treatments with E2 (ICV. ARC and VMH) animals were treated at 09:00 AM (one hour after the light cycle had commenced). Rats were killed by cervical dislocation. From each animal, the blood (for hormonal measurements), the whole hypothalamus, MBH, ARC, VMH, BAT, WAT, liver and muscle (for western blotting or malonyl-CoA assays) were immediately homogenized on ice to preserve

phosphorylated protein levels or the whole brain (for *in situ* hybridization) was dissected, and stored at -80°C until further processing. Dissection of the ARC and VMH was performed by micropunches under the microscope, as previously shown (López et al., 2010; Varela et al., 2012). The specificity of the ARC and VMH dissection was confirmed by analyzing the mRNA of their specific markers, namely SF1 and POMC (**Supplementary Figure 4A**).

### **Energy expenditure, locomotor activity, respiratory quotient, lipid utilization and nuclear magnetic resonance analysis**

Rats were analyzed for energy expenditure (EE), respiratory quotient (RQ) and locomotor activity (LA) using a calorimetric system (*LabMaster; TSE Systems; Bad Homburg, Germany*), as previously shown (Nogueiras et al., 2007; Martínez de Morentin et al., 2012; Imbernon et al., 2013). Rats were placed for adaptation for 1 week before starting the measurements. For the measurement of body composition, we used the nuclear magnetic resonance (NMR) imaging (*Whole Body Composition Analyzer; EchoMRI; Houston, TX*), as previously shown (López et al., 2010; Martínez de Morentin et al., 2012; Imbernon et al., 2013).

### **Sympathetic nerve activity recording**

Multi-fiber recording of sympathetic nerve activity (SNA) was obtained from the nerve subserving BAT, as previously described (Rahmouni et al., 2004; López et al., 2010; Whittle et al., 2012; Imbernon et al., 2013). Briefly, anesthesia was induced with ketamine/xylazine (91/9.1 mg/kg) and sustained with intravenous administration of  $\alpha$ -chloralose (initial dose: 25 mg/kg; sustaining dose of 6mg/kg/h). Each rat, equipped with ICV cannula 1 week earlier, was intubated (PE-50) to allow for spontaneous

respiration of oxygen-enriched room air. Body temperature was kept constant at 37.5° C with a surgical heat lamp and a heat pad to ensure that the preparation is stable. The nerve subserving BAT was identified using a dissecting scope and then mounted on a bipolar 36-gauge platinum-iridium electrode (*Cooner Wire Co.*, Chadsworth, CA, US). The nerve electrodes were attached to a high-impedance probe (*HIP-511, Grass Instruments Co.*, Quincy, Ma, US). The signal was amplified 10<sup>5</sup> times with a Grass P5 AC preamplifier, and filtered at both low (100Hz) and high-frequency (1000Hz) cut-off. This amplified, filtered signal was then sent to a speaker system and oscilloscope (*Model 54501A, Hewlett-Packard Co.*, Palo Alto, Ca. US). The signal was also routed to a *MacLab* analogue-digital converter (*Model 8S, Ad Instruments*, Castle Hill, New South Wales, Australia) for a permanent recording and data analysis on a *Macintosh* computer. Baseline BAT SNA was measured during a 10 min control period before a bolus ICV injection of vehicle or E2 was performed. The BAT SNA response to vehicle or E2 was followed for 6 hours. Background noise was excluded in the assessments of BAT SNA by correcting for post-mortem activity. SNA was expressed as a percent change from baseline.

### **Temperature measurements**

Body temperature was recorded twice at the end of the treatments with a rectal probe connected to digital thermometer (*BAT-12 Microprobe-Thermometer; Physitemp*; NJ, US). Skin temperature surrounding BAT was recorded with an infrared camera (*E60bx: Compact-Infrared-Thermal-Imaging-Camera; FLIR*; West Malling, Kent, UK) and analyzed with a specific software package (*FLIR-Tools-Software; FLIR*; West Malling, Kent, UK) (Martínez de Morentin et al., 2012; Whittle et al., 2012;

Schneeberger et al., 2013). The skin temperature surrounding BAT for each particular animal was calculated as the average temperature recorded by analyzing 6 pictures.

### **Hormone measurements**

Absence of gonadal function was confirmed by increased LH serum levels measured using a double-antibody method and radioimmunoassay kits (supplied by *Dr. AF Parlow; National Institute of Diabetes and Digestive and Kidney Diseases National Hormone and Peptide Program*, Torrance, CA) as reported (Vigo et al., 2007; Roa et al., 2009). Rat LH-I-10 was labeled in-house with <sup>125</sup>I using *Iodo-gen® tubes* (Pierce; Rockford, IL, US). Hormone concentrations were expressed using the reference preparation LH-RP-3. The intra- and inter-assay coefficients of variation (CVs) were <8% and <10%, respectively. Circulating E2 levels were determined using a commercial ultra-sensitive RIA kit (*Beckman Coulter*; Brea, CA, US). The sensitivity of the assay was 2.2 pg/mL, and the intra- and inter-assay CVs were 8.9% and 12.2%, respectively.

### **Malonyl-CoA assay**

The malonyl-CoA assays were performed as described (López et al., 2006; López et al., 2008; López et al., 2010).

### **Real-time quantitative PCR**

Real-time PCR (*TaqMan®*, Applied Biosystems; Foster City, CA, USA; or *SYBR® Green*, Roche Molecular Biochemicals, Mannheim, Germany, for the BAT samples from the microdialysis experiments) was performed using specific primers and probes (**Table S1**) as previously described (López et al., 2010; Martínez de Morentin et

al., 2012; Whittle et al., 2012). Values were expressed in relation to hypoxanthine-guanine phosphoribosyl-transferase (HPRT) levels.

### **In situ hybridization**

Coronal brain sections (16  $\mu$ m) were probed with a specific oligonucleotide for NPY (*GenBank Accession Number*: M20373; 5'-AGA TGA GAT GTG GGG GGA AAC TAG GAA AAG TCA GGA GAG CAA GTT TCA TT-3') and POMC (*GenBank Accession Number*: AF510391; 5'-CTT GAT GAT GGC GTT CTT GAA GAG CGT CAC CAG GGG CGT CTG GCT CTT-3') as previously published (López et al., 2006; López et al., 2008; Lage et al., 2010; López et al., 2010; Martínez de Morentin et al., 2012; Varela et al., 2012; Whittle et al., 2012). Sections were scanned and the hybridization signal was quantified by densitometry using *ImageJ-1.33* (NIH; Bethesda, MD, USA). We used between 16-20 sections for each animal (4-5 slides with four sections per slide). The mean of these 16-20 values was used as the densitometry value for each animal.

### **Western blotting**

Hypothalamic, ARC and VMH protein lysates were subjected to SDS-PAGE, electrotransferred on a PVDF membrane and probed with the following antibodies: ACC, pACC-Ser<sup>79</sup>, AMPK $\alpha$ 1, AMPK $\alpha$ 2 (*Upstate*; Temecula, CA, USA); FAS (*BD*; Franklin Lakes, NJ, USA), AKT, pAKT-Ser<sup>473</sup>, pAMPK-Thr<sup>172</sup>, Il-1 $\beta$ , pLKB1-Ser<sup>428</sup>, PI3K, pPI3K-Tyr<sup>199</sup>, STAT3, TNF $\alpha$  (*Cell Signaling*; Danvers; MA, USA);  $\alpha$ -tubulin,  $\beta$ -actin (*Sigma*; St. Louis, MO, USA), IL-6, UCP1, pSTAT3-Tyr<sup>705</sup> (*Abcam*; Cambridge, UK), CaMKK $\alpha$ , CaMKK $\beta$ , PP2C $\alpha$ , (*Santa Cruz*; Santa Cruz, CA, USA) as previously described (López et al., 2006; López et al., 2008; Roa et al., 2009; Lage et al., 2010;

López et al., 2010; Martínez de Morentin et al., 2012; Varela et al., 2012; Whittle et al., 2012; Imbernon et al., 2013). Values were expressed in relation to  $\alpha$ -tubulin (for BAT),  $\beta$ -actin (hypothalamus) protein levels.

### **Immunohistochemistry**

Enzymatic immunohistochemistry (*Dako EnVision<sup>TM</sup>+* system, peroxidase; Glostrup, Denmark), immunofluorescence and double labeling were performed as described (López et al., 2008; López et al., 2010; Varela et al., 2012; Whittle et al., 2012), using a rabbit anti-c-FOS (*Santa Cruz Biotechnology, CA, USA*). c-FOS positive cells were counted by using *ImageJ-1.33* (*NIH; Bethesda, MD, USA*). Five animals per experimental group were used and 7-11 image sections were bilaterally analyzed per animal. Toluidine blue staining was performed as previously reported (Varela et al., 2012). Detection of GFP was performed with an immunofluorescence procedure, using a rabbit anti-GFP (1:200; *Abcam; Cambridge, UK*). Detection was done with an anti-rabbit antibody conjugated with *Alexa 488* (1:200; *Molecular Probes; Grand Island, NY, US*) as previously reported (López et al., 2008; López et al., 2010; Varela et al., 2012; Whittle et al., 2012; Imbernon et al., 2013).

## SUPPLEMENTAL REFERENCES

Imbernon, M., Beiroa, D., Vazquez, M.J., Morgan, D.A., Veyrat-Durebex, C., Porteiro, B., Diaz-Arteaga, A., Senra, A., Busquets, S., Velasquez, D.A., Al-Massadi, O., Varela, L., Gandara, M., Lopez-Soriano, F.J., Gallego, R., Seoane, L.M., Argiles, J.M., López, M., Davis, R.J., Sabio, G., Rohner-Jeanrenaud, F., Rahmouni, K., Diéguez, C., and Nogueiras, R. (2013). Central Melanin-Concentrating Hormone Influences Liver and Adipose Metabolism Via Specific Hypothalamic Nuclei and Efferent Autonomic/JNK1 Pathways. *Gastroenterology* *144*, 636-649.

Lage, R., Vázquez, M.J., Varela, L., Saha, A.K., Vidal-Puig, A., Nogueiras, R., Diéguez, C., and López, M. (2010). Ghrelin effects on neuropeptides in the rat hypothalamus depend on fatty acid metabolism actions on BSX but not on gender. *FASEB J.* *24*, 2670-2679.

Liu, J., Bisschop, P.H., Eggels, L., Foppen, E., Ackermans, M.T., Zhou, J.N., Fliers, E., and Kalsbeek, A. (2013). Intrahypothalamic estradiol regulates glucose metabolism via the sympathetic nervous system in female rats. *Diabetes* *62*, 435-443.

López, M., Lage, R., Saha, A.K., Pérez-Tilve, D., Vázquez, M.J., Varela, L., Sangiao-Alvarellos, S., Tovar, S., Raghay, K., Rodríguez-Cuenca, S., Deoliveira, R.M., Castañeda, T., Datta, R., Dong, J.Z., Culler, M., Sleeman, M.W., Álvarez, C.V., Gallego, R., Lelliott, C.J., Carling, D., Tschop, M.H., Diéguez, C., and Vidal-Puig, A. (2008). Hypothalamic fatty acid metabolism mediates the orexigenic action of ghrelin. *Cell Metab* *7*, 389-399.

López, M., Lelliott, C.J., Tovar, S., Kimber, W., Gallego, R., Virtue, S., Blount, M., Vázquez, M.J., Finer, N., Powles, T., O'Rahilly, S., Saha, A.K., Diéguez, C., and Vidal-Puig, A.J. (2006). Tamoxifen-induced anorexia is associated with fatty acid synthase inhibition in the ventromedial nucleus of the hypothalamus and accumulation of malonyl-CoA. *Diabetes* *55*, 1327-1336.

López, M., Varela, L., Vázquez, M.J., Rodríguez-Cuenca, S., González, C.R., Velagapudi, V.R., Morgan, D.A., Schoenmakers, E., Agassandian, K., Lage, R., de Morentin, P.B., Tovar, S., Nogueiras, R., Carling, D., Lelliott, C., Gallego, R., Oresic, M., Chatterjee, K., Saha, A.K., Rahmouni, K., Diéguez, C., and Vidal-Puig, A. (2010). Hypothalamic AMPK and fatty acid metabolism mediate thyroid regulation of energy balance. *Nat. Med.* *16*, 1001-1008.

Martínez de Morentin, P.B., Whittle, A.J., Ferno, J., Nogueiras, R., Diéguez, C., Vidal-Puig, A., and López, M. (2012). Nicotine induces negative energy balance through hypothalamic AMP-activated protein kinase. *Diabetes* *61*, 807-817.

Nogueiras, R., Wiedmer, P., Perez-Tilve, D., Veyrat-Durebex, C., Keogh, J.M., Sutton, G.M., Pfluger, P.T., Castaneda, T.R., Neschen, S., Hofmann, S.M., Howles, P.N., Morgan, D.A., Benoit, S.C., Szanto, I., Schrott, B., Schurmann, A., Joost, H.G., Hammond, C., Hui, D.Y., Woods, S.C., Rahmouni, K., Butler, A.A., Farooqi, I.S., O'rahilly, S., Rohner-Jeanrenaud, F., and Tschop, M.H. (2007). The central melanocortin system directly controls peripheral lipid metabolism. *J. Clin. Invest* *117*, 3475-3488.

Rahmouni, K., Morgan, D.A., Morgan, G.M., Liu, X., Sigmund, C.D., Mark, A.L., and Haynes, W.G. (2004). Hypothalamic PI3K and MAPK differentially mediate regional sympathetic activation to insulin. *J. Clin. Invest* *114*, 652-658.

Roa, J., García-Galiano, D., Varela, L., Sánchez-Garrido, M.A., Pineda, R., Castellano, J.M., Ruíz-Pino, F., Romero, M., Aguilar, E., López, M., Gaytan, F., Diéguez, C., Pinilla, L., and Tena-Sempere, M. (2009). The mammalian target of rapamycin as novel central regulator of puberty onset via modulation of hypothalamic Kiss1 system. *Endocrinology* *150*, 5016-5026.

Schneeberger, M., Dietrich, M.O., Sebastian, D., Imbernon, M., Castano, C., Garcia, A., Esteban, Y., Gonzalez-Franquesa, A., Rodriguez, I.C., Bortolozzi, A., Garcia-Roves, P.M., Gomis, R., Nogueiras, R., Horvath, T.L., Zorzano, A., and Claret, M. (2013). Mitofusin 2 in POMC neurons connects ER stress with leptin resistance and energy imbalance. *Cell* *155*, 172-187.

Varela, L., Martínez-Sánchez N., Gallego, R., Vázquez, M.J., Roa, J., Gándara M., Schoenmakers, E., Nogueiras, R., Chatterjee, K., Tena-Sempere, M., Diéguez C, and López M (2012). Hypothalamic mTOR pathway mediates thyroid hormone-induced hyperphagia in hyperthyroidism. *J. Pathol.* 227, 209-222.

Vigo, E., Roa, J., Lopez, M., Castellano, J.M., Fernandez-Fernandez, R., Navarro, V.M., Pineda, R., Aguilar, E., Dieguez, C., Pinilla, L., and Tena-Sempere, M. (2007). Neuromedin s as novel putative regulator of luteinizing hormone secretion. *Endocrinology* 148, 813-823.

Whittle, A.J., Carobbio S, Martíns L, Slawik, M., Hondares, E., Vázquez, M.J., Morgan D, Csikasz, RI, Gallego, R., Rodriguez-Cuenca, S., Dale, M., Virtue, S., Villarroya, F., Cannon, B., Rahmouni, K., López M, and Vidal-Puig, A. (2012). Bmp8b increases brown adipose tissue thermogenesis through both central and peripheral actions. *Cell* 149, 871-885.